Journal of Molecular Catalysis A: Chemical 345 (2011) 90–95

Contents lists available at ScienceDirect

Journal of Molecular Catalysis A: Chemical

journal homepage: www.elsevier.com/locate/molcata

g-C_3N_4/SiO_2–HNb_3O_8 composites with enhanced photocatalytic activities for rhodamine B degradation under visible light

Huiqi Pan[a,b,c], Xiukai Li[a,b,c,*], Zongjin Zhuang[a,b,c], Chi Zhang[a,b,c,*]

[a] China-Australia Joint Research Center for Functional Molecular Materials, Jiangsu University, Zhenjiang 212013, PR China
[b] Scientific Research Academy, Jiangsu University, Zhenjiang 212013, PR China
[c] School of Chemistry and Chemical Engineering, Jiangsu University, Zhenjiang 212013, PR China

ARTICLE INFO

Article history:
Received 2 March 2011
Received in revised form 25 May 2011
Accepted 26 May 2011
Available online 2 June 2011

Keywords:
Photocatalysis
Visible light
Niobic acid
g-C_3N_4
Composite

ABSTRACT

Visible light-responsive g-C_3N_4/SiO_2–HNb_3O_8 composite photocatalysts were prepared by a solid state-reaction method with melamine as a g-C_3N_4 precursor. The photocatalytic activities of the samples were evaluated for rhodamine B (RhB) degradation under visible light irradiation and the results were compared with those obtained over pure SiO_2–HNb_3O_8 and g-C_3N_4. Techniques such as XRD, FT-IR, SEM, TEM, and UV–vis diffuse reflectance spectroscopy were adopted to explore the characteristics of samples. The g-C_3N_4/SiO_2–HNb_3O_8 composite materials exhibited superior activities than pure SiO_2–HNb_3O_8 and g-C_3N_4; the sample prepared with SiO_2–HNb_3O_8 to melamine ratio being 1:2 and the heating duration being 4 h performed the best. The improved activity of g-C_3N_4/SiO_2–HNb_3O_8 is attributed to the unique synergetic effect between SiO_2–HNb_3O_8 and g-C_3N_4.

1. Introduction

Semiconductor photocatalysis is a promising technique for environmental protection and solar energy conversion [1–5]. The photocatalytic degradation of harmful organic compounds is of particular interest [6–10]. As the photogenerated holes and electrons are essentially oxidation and reduction species, respectively, some organic contaminants could be completely decomposed over a photocatalyst with strong oxidation–reduction power [4,8,11]. Many Ti- and Nb-based metal oxides (e.g. TiO_2, Nb_2O_5) show photocatalytic activities in the UV range. Since UV-light accounts for only 4% in the whole solar spectrum, it is desirable to modify the photocatalysts for visible light application [12–16]. Lamellar titanates and niobates (e.g. $K_2Ti_4O_9$ and KNb_3O_8) are one unique type of metal oxides, which have layered crystal structures constructed by metal–oxygen polyhedrons. Previous research demonstrated that the acid phases of lamellar titanates and niobates could show much higher photocatalytic activities than their corresponding salt phases and simple TiO_2 and Nb_2O_5 [17–20]. It was proposed that the layered configuration should promote the migration of photoexcited electrons and holes, and that the interlayer space could provide more reaction active sites [21–23]. HNb_3O_8 is a typical lamellar niobic acid and shows fairly good visible light-responsive photocatalytic activity when the sample was doped with nitrogen [24]. However, like most protonic solid acids, HNb_3O_8 has rather low thermal stability and decomposes to the simple metal oxides at temperatures above 473 K [25]. SiO_2 pillared HNb_3O_8 (SiO_2–HNb_3O_8) could have a higher thermal stability exceeding 973 K [26]. The pillared materials also have expanded interlayer distance and therefore remarkable specific surface area, which may make the electrons transfer easier and provide more reaction active sites [26].

Graphitic carbon nitride (g-C_3N_4) is a novel metal-free photocatalyst with a band gap of ca. 2.8 eV. It is active for water reduction into H_2 or water oxidation into O_2 in the presence of a proper sacrificial reagent under visible light irradiation [27]. There was report that g-C_3N_4 is also active for the degradation of some organic dyes such as methyl orange [28]. g-C_3N_4 can also acts as a sensitizer, and g-C_3N_4 sensitized tantalic acids could show higher activity for hydrogen generation from aqueous methanol solution than pure g-C_3N_4 and tantalic acid [29]. Several precursors, such as cyanamide, dicyandiamide, urea, and melamine, have been used to obtain the g-C_3N_4 solids [30]. Compared with the former two precursors, urea and melamine are non-toxic and cheap [31].

Pillared solid acids have mesoporous characters and their large interlayer space make it possible to accommodate some guest materials. In view of the unique photoelectric properties of g-C_3N_4 and SiO_2–HNb_3O_8, we envisage that there might be certain

* Corresponding authors at: China-Australia Joint Research Center for Functional Molecular Materials, Jiangsu University, Zhenjiang 212013, PR China.
Tel.: +86 511 88797815; fax: +86 511 88797815.
E-mail addresses: li.xiukai@gmail.com (X. Li), chizhang@ujs.edu.cn (C. Zhang).

1381-1169/$ – see front matter © 2011 Elsevier B.V. All rights reserved.
doi:10.1016/j.molcata.2011.05.024

synergism between the two materials if the g-C_3N_4/SiO_2–HNb_3O_8 heterojunction could be successfully fabricated. In the present study, serial g-C_3N_4/SiO_2–HNb_3O_8 composites with different g-C_3N_4 loading were therefore prepared. The physico-chemical properties and the photocatalytic activities of samples were investigated in detail; the structure–performance relationships were proposed and discussed.

2. Experimental

2.1. Catalyst preparation

The HNb_3O_8 solid acid was prepared by the proton-exchange reaction with KNb_3O_8 as a precursor [26,32]. KNb_3O_8 was prepared by heating stoichiometric amounts of K_2CO_3 and Nb_2O_5 at 900 °C for 10 h. The SiO_2 pillared HNb_3O_8 sample was prepared by the two-step ion-exchange method with *n*-dodecylamine and tetraethyl orthosilicate (TEOS) as respectively the pre-expanding reagent and silicon source [26]. The TEOS intercalated HNb_3O_8 was calcined at 500 °C for 4 h for the formation of SiO_2 pillared HNb_3O_8 (designated as SiO_2–HNb_3O_8). The g-C_3N_4/SiO_2–HNb_3O_8 composites were prepared by heating certain proportion of SiO_2–HNb_3O_8 and melamine in air at 500 °C for different durations. The samples were designated as g-C_3N_4/SiO_2–HNb_3O_8(*a*:*b* *x* h), where *a*:*b* means the mass ratio of SiO_2–HNb_3O_8 to melamine, while *x* means the heating time. Pure g-C_3N_4 was prepared by heating melamine alone in air at 500 °C for 4 h.

2.2. Sample characterization

The phase compositions of samples were identified by X-ray Powder Diffraction (Cu K_α radiation, Bruker AXS-D8) in the 2θ range of 1–80°. FT-IR spectra of the samples were collected on a Nicolet Nexus 470 FT-IR spectrophotometer at room temperature by KBr method. Morphologies of samples were characterized using a scanning electron microscope (JSM-7001F, JEOL) and a high resolution transmission electron microscope (HR JEM-2100, JEOL). The UV–vis diffuse reflectance spectra were recorded at room temperature on a Shimadzu UV-2450 UV–vis spectrometer with barium sulfate as the reference sample.

2.3. Activity test

For the evaluation of catalytic activity, 0.2 g catalyst was suspended in 100 ml rhodamine B (RhB) aqueous solution (6.0 mg l^{-1}, pH value: 7) in a pyrex reactor. The suspension was stirred in the dark for about 40 min before light was turned on. A 350 W Xe-lamp (Nanshen Company, Shanghai) equipped with UV cutoff filter ($\lambda > 400$ nm) and a water filter was used as light source. The average intensity of the incident light was ca. 50.0 mW cm^{-2}. At given irradiation time intervals, ca. 3.0 ml of the reaction suspension was sampled, and separated by filtration. The concentration of RhB was determined by monitoring the changes in the absorbance maximized at ca. 554 nm.

3. Results and discussion

3.1. Characterization

HNb_3O_8 is a typical lamellar niobic acid that crystallizes in an orthorhombic symmetry [24,26]. It has layered structures constructed by 2D $Nb_3O_8^-$ anion slices built by corner- and edge-sharing NbO_6 octahedra, the H^+ cations are located between the slices. The interlayer spacing of HNb_3O_8 is only 3.8 Å [24–26], thus it is difficult for the reactants to access the active reaction sites at the interlayer surface. Inorganic materials such as SiO_2, TiO_2 and Al_2O_3 could serve as pillars to expand the interlayer distances of lamellar solid acids. The pillared samples could have interlayer distances up to tens of angstrom and therefore show mesoporous characters. Fig. 1 shows the XRD patterns of HNb_3O_8 and g-C_3N_4/SiO_2–HNb_3O_8 composites obtained by heating SiO_2–HNb_3O_8 with melamine under different conditions. The 0 2 0 diffraction peak at $2\theta = 7.8°$ for HNb_3O_8 (Fig. 1a) is characteristic of the layered structure of the sample, and the *d* value (ca. 11.3 Å) corresponds to the interlayer distance. From Fig. 1b one can see that the 0 2 0 diffraction peak for SiO_2–HNb_3O_8 shift remarkably to $2\theta = 3.7°$ (corresponds to a *d* value of 30.2 Å). In view that the thickness of the $Nb_3O_8^-$ anion slices is 7.5 Å [26], the interlayer spacing of SiO_2–HNb_3O_8 is expanded to 22.7 Å (30.2 Å subtract 7.5 Å); this value is almost 6 times of that (3.8 Å) of HNb_3O_8. In accordance, the surface area value was increased from 7.2 m^2 g^{-1} of non-pillared HNb_3O_8 to 220.1 m^2 g^{-1} of SiO_2–HNb_3O_8. The g-C_3N_4 sample prepared from direct melamine decomposition shows intense diffraction peak at $2\theta = 27.7°$ (Fig. 1j), which is consistent with that reported in literature [29,31]. The melamine to SiO_2–HNb_3O_8 ratio and the heating duration is crucial for the amount of g-C_3N_4 loading and could have significant impact on the structure of SiO_2–HNb_3O_8. From Table 1 one can see that the amount of g-C_3N_4 loading increases with melamine to SiO_2–HNb_3O_8 ratio but decreases with the heating time. The loading of g-C_3N_4 is almost zero for the g-C_3N_4/SiO_2–HNb_3O_8 (1:2, 5 h) sample. It was demonstrated that g-C_3N_4 could be oxidatively decomposed to nitrogen and cyano fragments very quickly in the air atmosphere [31]. In the present study, the deammonation of melamine created an ammonia atmosphere in the semiclosed system and this suppressed the combustion of the g-C_3N_4 product. After the deammonation process, the ammonia concentration in the semiclosed system decreased while the concentration of air increased, as a result the g-C_3N_4 product oxidatively decomposed quickly and the amount of g-C_3N_4 loading decreased accordingly. It was also noted that the formation of g-C_3N_4 species favors the stability of SiO_2–HNb_3O_8, and this effect depends on the amount of g-C_3N_4 loaded. For the g-C_3N_4/SiO_2–HNb_3O_8 (1:1.5, 4 h) and g-C_3N_4/SiO_2–HNb_3O_8 (1:2, 5 h) samples those with very low g-C_3N_4 loadings, the 0 2 0 diffraction peaks are very weak, signifying that the layered structure of SiO_2–HNb_3O_8 was partially destroyed. The diffraction peak of

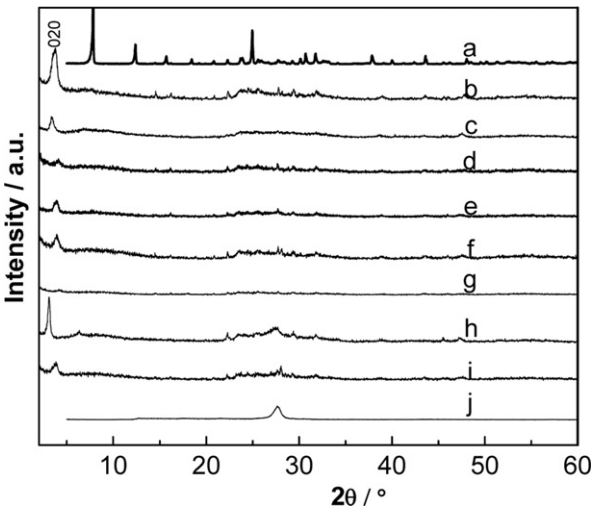

Fig. 1. XRD patterns of (a) HNb_3O_8; (b) SiO_2–HNb_3O_8; (c) g-C_3N_4/SiO_2–HNb_3O_8 (1:1.5, 2 h); (d) g-C_3N_4/SiO_2–HNb_3O_8 (1:1.5, 4 h); (e) g-C_3N_4/SiO_2–HNb_3O_8 (1:2, 2 h); (f) g-C_3N_4/SiO_2–HNb_3O_8 (1:2, 4 h); (g) g-C_3N_4/SiO_2–HNb_3O_8 (1:2, 5 h); (h) g-C_3N_4/SiO_2–HNb_3O_8 (1:3, 2 h); (i) g-C_3N_4/SiO_2–HNb_3O_8 (1:3, 4 h) and (j) pure g-C_3N_4 prepared by heating melamine at 500 °C for 4 h.

Table 1
The preparation conditions and physical characteristics of samples.

Sample	Solid acid/melamine	Heating condition	g-C_3N_4 loading (wt.%)[a]	Band gap (eV)
SiO_2–HNb_3O_8	–	–	0	3.06
g-C_3N_4/SiO_2–HNb_3O_8	1:1.5	500 °C, 2 h	17.4	2.47
g-C_3N_4/SiO_2–HNb_3O_8	1:1.5	500 °C, 4 h	6.5	2.79
g-C_3N_4/SiO_2–HNb_3O_8	1:2	500 °C, 2 h	29.0	2.41
g-C_3N_4/SiO_2–HNb_3O_8	1:2	500 °C, 4 h	28.6	2.48
g-C_3N_4/SiO_2–HNb_3O_8	1:2	500 °C, 5 h	~0.0	2.82
g-C_3N_4/SiO_2–HNb_3O_8	1:3	500 °C, 2 h	54.9	2.46
g-C_3N_4/SiO_2–HNb_3O_8	1:3	500 °C, 4 h	44.4	2.46
g-C_3N_4	–	500 °C, 4 h	100.0	2.53

[a] The weight loading of g-C_3N_4. The data was obtained according to: g-C_3N_4 loading = W(g-C_3N_4)/[W(g-C_3N_4) + W(SiO_2–HNb_3O_8)] × 100%. W(g-C_3N_4): the weight of g-C_3N_4; W(SiO_2–HNb_3O_8): the weight of SiO_2–HNb_3O_8.

g-C_3N_4 could hardly be observed for the g-C_3N_4/SiO_2–HNb_3O_8 composites, except the g-C_3N_4/SiO_2–HNb_3O_8 (1:3, 2 h) sample with 54.9 wt.% g-C_3N_4 loading. Similarly, over TiO_2 supported g-C_3N_4, the diffraction peak of g-C_3N_4 was detected only when the loading of g-C_3N_4 exceed 50% [33]. It is likely that the supported g-C_3N_4 component was amorphous or was highly dispersed. In view that the interlayer spacing of SiO_2–HNb_3O_8 is as large as 30.2 Å, it is reasonable that there should be certain proportion of g-C_3N_4 present between the interlayer of SiO_2–HNb_3O_8.

The Fourier transform infrared (FT-IR) spectra of the g-C_3N_4/SiO_2–HNb_3O_8 composites as well as those of the two component materials are shown in Fig. 2. For the pure g-C_3N_4 sample (Fig. 2i), absorptions attributable to the vibration of the CN heterocycles could be clearly observed in the range of 1200–1650 cm^{-1} [34]; the characteristic breathing mode of the triazine units and the stretching vibration modes of NH were also observed at respectively around 808 cm^{-1} and 3000 cm^{-1} [35]. This observation indicates that the amino functions still existed in the g-C_3N_4 product after the heating process. The characteristic g-C_3N_4 absorptions were also observed over the g-C_3N_4/SiO_2–HNb_3O_8 composites, except the g-C_3N_4/SiO_2–HNb_3O_8 (1:1.5, 4 h) and g-C_3N_4/SiO_2–HNb_3O_8 (1:2, 5 h) samples with very low g-C_3N_4 loadings. The results of FT-IR are in good agreement with those of XRD, and support that g-C_3N_4 has been successfully loaded onto SiO_2–HNb_3O_8.

The particle sizes and the morphologies of the representative samples were examined by using SEM analyses. Fig. 3A shows the image of SiO_2–HNb_3O_8 powder containing a number of lamellar plates in micron size. The g-C_3N_4/SiO_2–HNb_3O_8 (1:2, 4 h) sample (Fig. 3B) looks fluffier than SiO_2–HNb_3O_8, probably because of g-C_3N_4 loading and the impact of gases discharged from melamine decomposition. The g-C_3N_4/SiO_2–HNb_3O_8 (1:1.5, 4 h) and g-C_3N_4/SiO_2–HNb_3O_8 (1:2, 5 h) samples (Fig. 3C and D) with low g-C_3N_4 loadings exhibited smooth particle surface compared with the g-C_3N_4/SiO_2–HNb_3O_8 (1:2, 4 h) sample. Transmission electron microscopy (TEM) was carried out to investigate the textures of SiO_2–HNb_3O_8 and g-C_3N_4/SiO_2–HNb_3O_8 (1:2, 4 h). One can see from Fig. 4 that both samples have layered structures. The interlayer spacing measured from the TEM image of SiO_2–HNb_3O_8 is about 2.3 nm, which is in accordance with the data (22.7 Å) obtained from XRD. As the layered structures were partially destroyed and could be hardly observed, the TEM images of g-C_3N_4/SiO_2–HNb_3O_8 (1:1.5, 4 h) and g-C_3N_4/SiO_2–HNb_3O_8 (1:2, 5 h) were not shown.

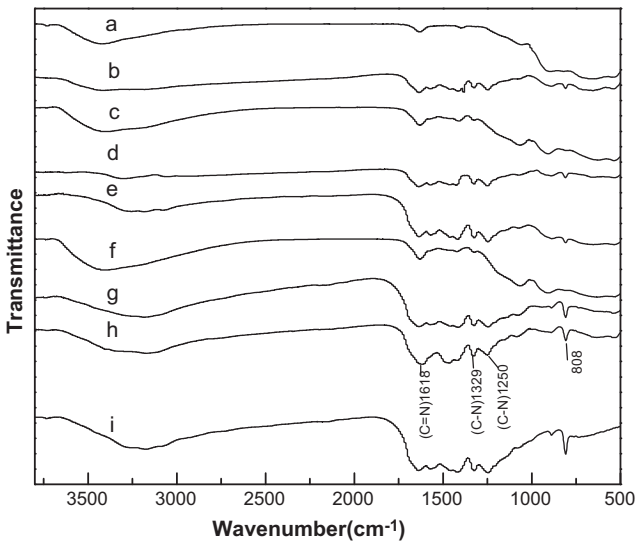

Fig. 2. FT-IR spectra of (a) SiO_2–HNb_3O_8; (b) g-C_3N_4/SiO_2–HNb_3O_8 (1:1.5, 2 h); (c) g-C_3N_4/SiO_2–HNb_3O_8 (1:1.5, 4 h); (d) g-C_3N_4/SiO_2–HNb_3O_8 (1:2, 2 h); (e) g-C_3N_4/SiO_2–HNb_3O_8 (1:2, 4 h); (f) g-C_3N_4/SiO_2–HNb_3O_8 (1:2, 5 h); (g) g-C_3N_4/SiO_2–HNb_3O_8 (1:3, 2 h); (h) g-C_3N_4/SiO_2–HNb_3O_8 (1:3, 4 h) and (i) g-C_3N_4.

The optical properties of the g-C_3N_4/SiO_2–HNb_3O_8 composites as well as pure g-C_3N_4 and SiO_2–HNb_3O_8 were investigated by UV–vis diffuse reflectance spectroscopy, and the results are shown in Fig. 5. The g-C_3N_4 sample is yellow colored and have absorption above 400 nm, while the white colored SiO_2–HNb_3O_8 sample only absorbs the UV light (λ < 400 nm). The g-C_3N_4/SiO_2–HNb_3O_8 composite materials, except the g-C_3N_4/SiO_2–HNb_3O_8 (1:1.5, 4 h) and g-C_3N_4/SiO_2–HNb_3O_8 (1:2, 5 h) samples with very low g-C_3N_4 loadings, have obvious light absorption in the visible region. Compared with the g-C_3N_4 sample, it is noted that the g-C_3N_4/SiO_2–HNb_3O_8 samples with high g-C_3N_4 loadings have more visible light absorption, probably because of the differences in preparation conditions and the dispersion of g-C_3N_4. The band-gap values were calculated from the sharp absorption edges of the spectra, and the data were listed in Table 1. The band gap values of g-C_3N_4/SiO_2–HNb_3O_8 composites vary from 2.4 to 2.8 eV, which are lower than that (3.1 eV) of SiO_2–HNb_3O_8. Previous research indicated that when amino group containing compound such as urea was used as nitrogen source, nitrogen could be easily doped into a niobic acid and a titanic acid through a simple solid state reaction that conducted at 400 °C [24,25]. In the present study, the preparation of g-C_3N_4/SiO_2–HNb_3O_8 was done by a similar method except that melamine was used as g-C_3N_4 precursor and nitrogen source, thus it is possible to deduce that certain amount of nitrogen atoms were also doped into the SiO_2–HNb_3O_8 moiety. However, as the surface of SiO_2–HNb_3O_8 was covered by g-C_3N_4, it is difficult to measure the state and amount of doped nitrogen by the XPS analysis.

3.2. Activity

The photocatalytic activity of the g-C_3N_4/SiO_2–HNb_3O_8 samples were evaluated for rhodamine B (RhB) photodegradation under visible light (λ > 400 nm) irradiation, and the results have been compared with RhB photolysis (without photocatalyst). One can see from Fig. 6 that the photolysis of RhB under visible light irradiation

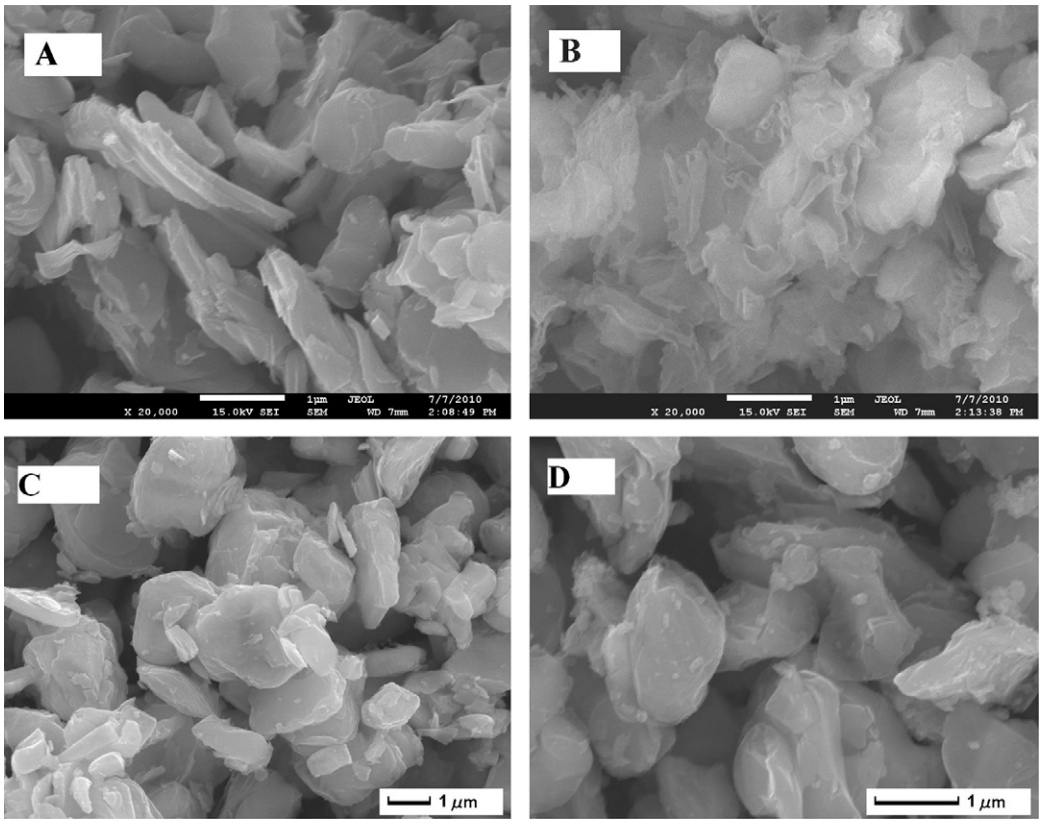

Fig. 3. SEM images of (A) SiO_2–HNb_3O_8; (B) g-C_3N_4/SiO_2–HNb_3O_8 (1:2, 4 h); (C) g-C_3N_4/SiO_2–HNb_3O_8 (1:1.5, 4 h) and (D) g-C_3N_4/SiO_2–HNb_3O_8 (1:2, 5 h). The scale bars represent 1 μm.

was very slow, and that only less than 5% of RhB was converted after 100 min of irradiation. When the g-C_3N_4/SiO_2–HNb_3O_8 samples were applied, the concentrations of RhB decreased remarkably with visible light irradiation. The g-C_3N_4/SiO_2–HNb_3O_8 (1:2, 4 h) and the g-C_3N_4/SiO_2–HNb_3O_8 (1:1.5, 2 h) samples performed much better than the other samples, over which approximately 97% of RhB was converted after 40 min of visible-light irradiation, while over the other composites the same extent of RhB degradation took more than 80 min. This activity is also much higher than those observed over pure SiO_2–HNb_3O_8 and g-C_3N_4. Fig. 7 shows the spectra of RhB photodegradation over g-C_3N_4/SiO_2–HNb_3O_8 (1:2, 4 h). One can see that not only did the main absorbance in the visible region decrease dramatically with irradiation, but also the peaks in the UV region decreased with irradiation time. It follows that the dye molecules had been degraded instead of being simply decolorized in the present study. Due to the fact that the crystallinity and the dispersion state of g-C_3N_4, and the interaction between the guest/host components might vary with different melamine to SiO_2–HNb_3O_8 ratios and different heating durations, certain samples prepared with different synthesis parameters displayed similar activities.

The excellent photocatalytic activity of g-C_3N_4/SiO_2–HNb_3O_8 composite should be ascribed to the synergism between the two component materials. The mechanism of RhB photodegradation over g-C_3N_4/SiO_2–HNb_3O_8 was illustrated in Fig. 8. g-C_3N_4 is a material with extremely high conduction band edge potentials (−1.12 eV [33]), the data is more negative than that of most titanates and niobates (e.g. −0.29 eV of TiO_2 [33], ca. 0.0 eV of Nb_2O_5 [36], −0.12 eV of $KNbO_3$ [37]). When the g-C_3N_4/SiO_2–HNb_3O_8

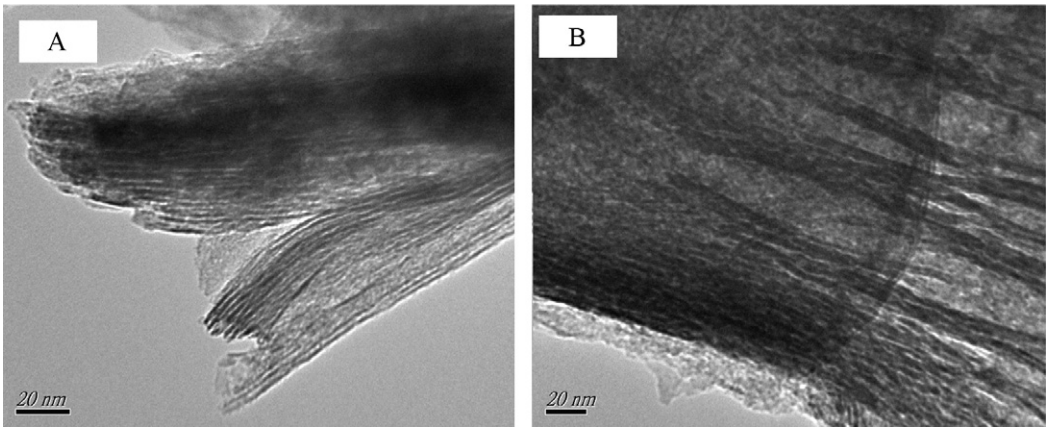

Fig. 4. TEM images of (A) SiO_2–HNb_3O_8 and (B) g-C_3N_4/SiO_2–HNb_3O_8 (1:2, 4 h).

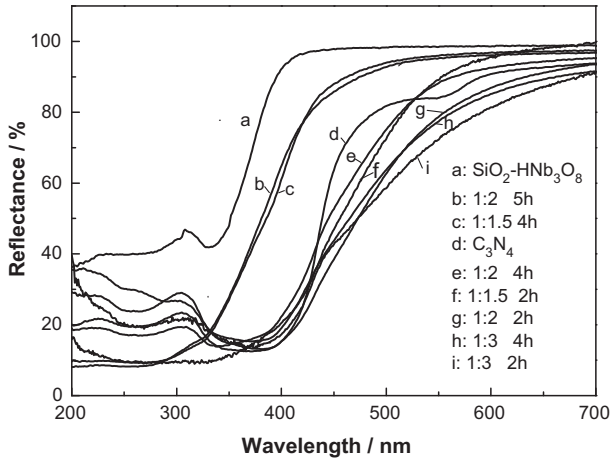

Fig. 5. UV–vis diffuse reflectance spectra of (a) SiO_2–HNb_3O_8; (b) g-C_3N_4/SiO_2–HNb_3O_8 (1:2, 5 h); (c) g-C_3N_4/SiO_2–HNb_3O_8 (1:1.5, 4 h); (d) g-C_3N_4; (e) g-C_3N_4/SiO_2–HNb_3O_8 (1:2, 4 h); (f) g-C_3N_4/SiO_2–HNb_3O_8 (1:1.5, 2 h); (g) g-C_3N_4/SiO_2–HNb_3O_8 (1:2, 2 h); (h) g-C_3N_4/SiO_2–HNb_3O_8 (1:3, 4 h) and (i) g-C_3N_4/SiO_2–HNb_3O_8 (1:3, 2 h).

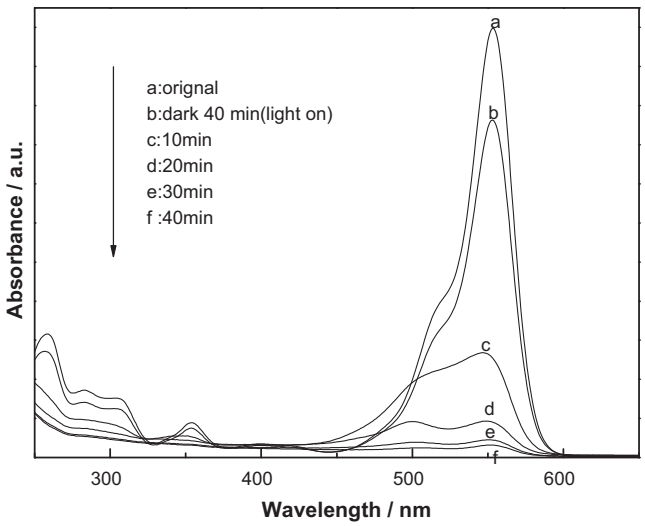

Fig. 7. The UV–vis spectroscopic changes of the RhB aqueous solution over the g-C_3N_4/SiO_2–HNb_3O_8 (1:2, 4 h) sample.

composite photocatalyst was irradiated under visible light, g-C_3N_4 and the nitrogen doped SiO_2–HNb_3O_8 were excited. Because of the g-C_3N_4/SiO_2–HNb_3O_8 heterojunction structure, the photogenerated electrons in g-C_3N_4 could transfer to the conduction band of SiO_2–HNb_3O_8 via the interface, while the holes at the valence band of SiO_2–HNb_3O_8 could transfer to g-C_3N_4. As mentioned above, SiO_2–HNb_3O_8 has layered crystal structure and its interlayer spacing is as large as 22.7 Å. Being a strong protonic acid, HNb_3O_8 is hygroscopic and could absorb the water molecules through hydrogen bonding [24,25]. The electrons and holes at the interlayer surface of the sample then react with the molecular oxygen and adsorbed H_2O to generate the $^{\bullet}O_2^-$ and $^{\bullet}OH$ reaction active species. The RhB dye was reduced by the photogenerated electrons or was oxidized by the active oxidation species (the holes, $^{\bullet}O_2^-$, and $^{\bullet}OH$). The quick separation and consumption of electrons and holes at the interlayer surface of SiO_2–HNb_3O_8 in turn facilitates the electron–hole pair separation in g-C_3N_4. When the pure g-C_3N_4

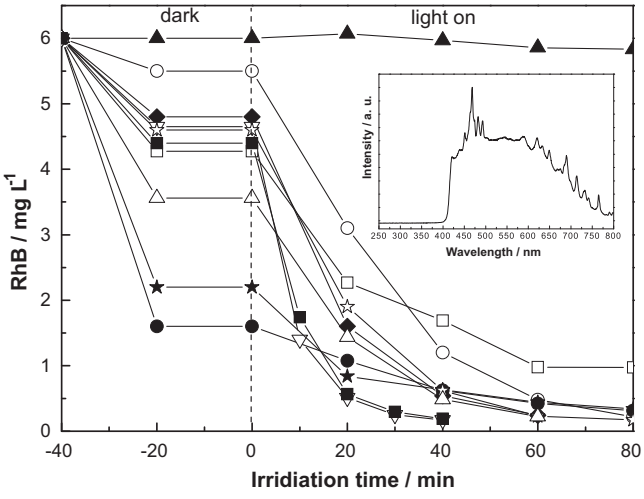

Fig. 6. The photocatalytic degradation of RhB over various photocatalysts under visible light (λ > 400 nm) irradiation. (▲) No catalyst; (○) g-C_3N_4; (●) SiO_2–HNb_3O_8; (▽) g-C_3N_4/SiO_2–HNb_3O_8 (1:2, 4 h); (☆) g-C_3N_4/SiO_2–HNb_3O_8 (1:3, 4 h); (★) g-C_3N_4/SiO_2–HNb_3O_8 (1:1.5, 4 h); (♦) g-C_3N_4/SiO_2–HNb_3O_8 (1:2, 2 h); (□) g-C_3N_4/SiO_2–HNb_3O_8 (1:2, 5 h); (△) g-C_3N_4/SiO_2–HNb_3O_8 (1:3, 2 h); (■) g-C_3N_4/SiO_2–HNb_3O_8 (1:1.5, 2 h). The inset shows the spectrum of the wavelength distribution of the irradiation light applied in activity test.

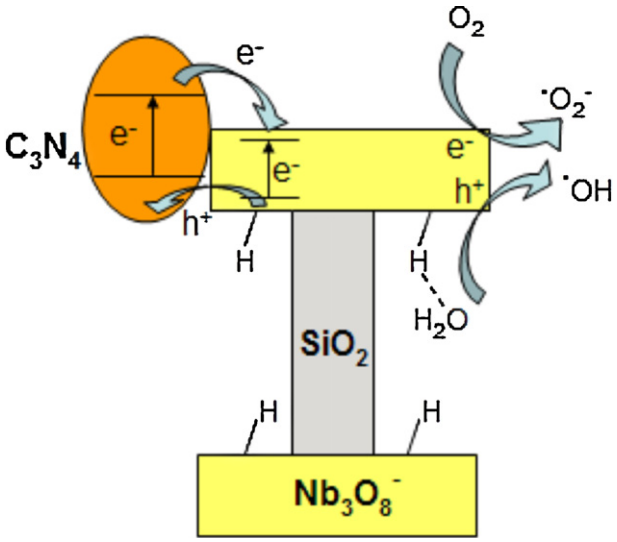

Fig. 8. The synergism between g-C_3N_4 and nitrogen doped SiO_2–HNb_3O_8.

was used solely as the photocatalyst for degradation of RhB, the efficiency of electron–hole pair separation was restricted and the observed activity was therefore lower. The enhanced photoactivities over heterojunctions have also been observed over a variety of composite materials such as CdS/TiO_2 [38], Co_3O_4/$BiVO_4$ [39], and $FeTiO_3$/TiO_2 [40]. The fabrication of heterojunctions also provides a possible method to develop visible light-responsive photocatalysts. In view of the unique photoelectric properties of lamellar solid acids, it is envisaged that new heterojunctions with novel photocatalytic activities could be prepared based on lamellar solid acids.

4. Conclusions

We demonstrated that the g-C_3N_4/SiO_2–HNb_3O_8 composite photocatalyst with enhanced visible light-responsive photocatalytic activity. The results of XRD and FT-IR analyses indicate that g-C_3N_4 has been successfully loaded onto SiO_2–HNb_3O_8. Smaller melamine to SiO_2–HNb_3O_8 mass ratio or longer heating time could lead to lower g-C_3N_4 loading. The intercalation of g-C_3N_4 helped to stabilize the layered structures of the solid acid during the ther-

mal process of sample preparation. The UV–vis diffuse reflectance spectra reveal that the g-C_3N_4/SiO_2–HNb_3O_8 samples absorb light in the visible region. The g-C_3N_4/SiO_2–HNb_3O_8 composites show superior activities than pure SiO_2–HNb_3O_8 and g-C_3N_4, and the sample prepared with SiO_2–HNb_3O_8 to melamine ratio being 1:2 and the heating duration being 4 h performed the best. The enhanced photocatalytic activity of g-C_3N_4/SiO_2–HNb_3O_8 composite is ascribed to the synergism between the two component materials. The unique photoelectric property and protonic acidity of SiO_2–HNb_3O_8 facilitate the electron–hole pair separation in the heterojunction system.

Acknowledgements

This research was supported by the National Natural Science Foundation of China (No. 21003064) and the Research Foundation of Jiangsu University (No. 1283000372/3).

References

[1] K. Maeda, K. Teramura, D. Lu, T. Takata, N. Saito, Y. Inoue, K. Domen, Nature 440 (2006) 295.
[2] N.Q. Wu, J. Wang, D. Tafen, H. Wang, J.G. Zheng, J.P. Lewis, X.G. Liu, S.S. Leonard, A. Manivannan, J. Am. Chem. Soc. 132 (2010) 6679–6685.
[3] R. Asahi, T. Morikawa, T. Ohwaki, K. Aoki, Y. Taga, Science 293 (2001) 269–271.
[4] X. Li, J. Ye, J. Phys. Chem. C 111 (2007) 13109–13116.
[5] X. Li, S. Ouyang, N. Kikugawa, J. Ye, Appl. Catal. A 334 (2008) 51–58.
[6] M.R. Hoffmann, S.T. Martin, W. Choi, D.W. Bahnemann, Chem. Rev. 95 (1995) 69–96.
[7] A.L. Linsebigler, G. Lu, J.T. Yates, Chem. Rev. 95 (1995) 735–758.
[8] J. Tang, Z. Zou, J. Ye, Angew. Chem. Int. Ed. 43 (2004) 4463–4466.
[9] D. Chatterjee, S. Dasgupta, J. Photochem. Photobiol. C 6 (2005) 186–205.
[10] H.G. Kim, D.W. Hwang, J.S. Lee, J. Am. Chem. Soc. 126 (2004) 8912–8913.
[11] S. Rodrigues, S. Uma, I.N. Martyanov, K.J. Klabunde, J. Catal. 233 (2005) 405–410.
[12] A. Fujishima, T.N. Rao, D.A. Tryk, J. Photochem. Photobiol. C 1 (2000) 1–21.
[13] T. Takata, A. Tanaka, M. Hara, J.N. Kondo, K. Domen, Catal. Today 44 (1998) 17–26.
[14] A. Iwase, H. Kato, A. Kudo, Catal. Lett. 108 (2006) 7–10.
[15] G. Zhang, J. Gong, X. Zou, F. He, H. Zhang, Q. Zhang, Y. Liu, X. Yang, B. Hu, Chem. Eng. J. 123 (2006) 59–64.
[16] Y. Inoue, T. Niiyama, Y. Asai, K. Sato, Chem. Commun. 1 (1992) 579–580.
[17] J. Yoshimura, Y. Ebina, J. Kondo, K. Domen, A. Tanaka, J. Phys. Chem. 97 (1993) 1970–1973.
[18] L. Zhang, W. Zhang, L. Lu, X. Yang, X. Wang, J. Mater. Sci. 41 (2006) 3917–3921.
[19] K. Domen, J. Yoshimura, T. Sekine, A. Tanakaa, T. Onishi, Catal. Lett. 4 (1990) 339–343.
[20] K. Domen, Y. Ebina, T. Sekine, A. Tanakaa, J. Kondo, C. Hirose, Catal. Today 16 (1993) 479–486.
[21] X. Wang, W. Hou, H. Wang, Q. Yan, Catal. Commun. 3 (2002) 275–280.
[22] X. Wang, W. Hou, Q. Yan, Chem. Lett. (2001) 188–189.
[23] S. Yin, D. Maeda, M. Ishitsuka, J. Wu, T. Sato, Solid State Ionics 151 (2002) 377–389.
[24] X. Li, N. Kikugawa, J. Ye, Adv. Mater. 20 (2008) 3816–3819.
[25] X. Li, N. Kikugawa, J. Ye, Chem. Eur. J. 15 (2009) 3538–3545.
[26] X. Guo, W. Hou, W. Ding, Y. Fan, Q. Yan, Y. Chen, Micropor. Mesopor. Mater. 80 (2005) 269–274.
[27] X.C. Wang, K. Maeda, A. Thomas, K. Takanabe, G. Xin, J.M. Carlsson, K. Domen, M. Antonietti, Nat. Mater. 8 (2009) 76–80.
[28] X.C. Wang, X.F. Chen, A. Thomas, X.Z. Fu, M. Antonietti, Adv. Mater. 21 (2009) 1–4.
[29] Q. Li, B. Yue, H. Iwai, T. Kako, J. Ye, J. Phys. Chem. C 114 (2010) 4100–4105.
[30] A. Thomas, A. Fischer, F. Goettmann, M. Antonietti, J. Muller, R. Schlogl, J.M. Carlsson, J. Mater. Chem. 18 (2008) 4893–4908.
[31] S.C. Yan, Z.S. Li, Z.G. Zou, Langmuir 25 (2009) 10397–10401.
[32] X. Jing, Y. Li, Q. Yang, Q. Yin, Mater. Sci. Eng. B 110 (2004) 18–22.
[33] H. Yan, H. Yang, J. Alloys Compd. 509 (2011) L26–L29.
[34] X.F. Li, J. Zhang, L.H. Shen, Y.M. Ma, W.W. Lei, Q.L. Cui, G.T. Zou, Appl. Phys. A: Mater. Sci. Process. 94 (2009) 387–392.
[35] M.J. Bojdys, J.O. Muller, M. Antonietti, A. Thomas, Chem. Eur. J. 14 (2008) 8177–8182.
[36] H. Kominami, K. Oki, M. Kohno, S. Onoue, Y. Kera, B. Ohtani, J. Mater. Chem. 11 (2001) 604–609.
[37] D.E. Scaife, Sol. Energy 25 (1980) 41–54.
[38] W.W. So, K.J. Kim, S.J. Moon, Int. J. Hydrogen Energy 29 (2004) 229–234.
[39] M. Long, W. Cai, J. Cai, B. Zhou, X. Chai, Y. Wu, J. Phys. Chem. B 110 (2006) 20211–20216.
[40] B. Gao, Y.J. Kim, A.K. Chakraborty, W.I. Lee, Appl. Catal. B 83 (2008) 202–207.